Connectivity of somatosensory cortical area 1 form an anatomical substrate for the emergence of multifinger receptive fields and complex feature selectivity in the squirrel monkey (Saimiri sciureus)

Journal:	*Journal of Comparative Neurology*
Manuscript ID:	JCN-13-0228.R2
Wiley - Manuscript type:	Research Article
Keywords:	touch, tract tracing, optical imaging, cortical hierarchy, primate

SCHOLARONE™
Manuscripts

For Peer Review

Connectivity of somatosensory cortical area 1 form an anatomical substrate for the emergence of multifinger receptive fields and complex feature selectivity in the squirrel monkey (*Saimiri sciureus)*

Mária Ashaber[1,2], Emese Pálfi[1,2], Robert M. Friedman[3], Cory Palmer[4], Balázs Jákli[5], Li Min Chen[6], Orsolya Kántor[2], Anna W. Roe[3*], László Négyessy[1,2*]

[1]Department of Theory, Institute for Particle and Nuclear Physics, Wigner Research Centre for Physics, Hungarian Academy of Sciences, Budapest, H-1121 Hungary, [2]Department of Anatomy, Histology and Embryology, Semmelweis University Medical School, Budapest, H-1094 Hungary, [3]Department of Psychology, Vanderbilt University, Nashville, TN 37240-7817 USA, [4]Department of Mathematics, University of Illinois, Urbana-Champaign, Urbana, IL 61801 USA, [5]Faculty of Information Technology, Pázmány Péter Catholic University, Budapest, H-1083 Hungary, [6]Department of Radiology and Radiological Science, Institute of Imaging Science, Vanderbilt University Medical Center, Nashville, TN 37232 USA

Running title: Connections of area 1 fingertip representations

Keywords: cortical hierarchy, optical imaging, touch, tract tracing, primate

***Corresponding authors:**

László Négyessy, Department of Theory, Institute for Particle and

For Peer Review

Nuclear Physics, Wigner Research Centre for Physics, Hungarian Academy of Sciences, P.O. Box 49, Budapest, H-1525 Hungary. E-mail: negyessy.laszlo@wigner.mta.hu

Anna W. Roe, Department of Psychology, Vanderbilt University, Nashville, TN 37240-7817 USA. E-mail: anna.roe@vanderbilt.edu

Funding. This study was supported by FIRCA NS059061 (to A.W.R. and L.N.), NS044375 (to A.W.R.) and the Hungarian Scientific Research Fund OTKA NN79366 (to L.N.).

For Peer Review

Abstract

Converging evidence shows that interaction of digit specific input, which is required to form global tactile percepts, begins as early as area 3b in the primary somatosensory cortex with the involvement of intrinsic lateral connections. How tactile processing is further elaborated in area 1, the next stage of the somatosensory cortical hierarchy, is less understood. This question was investigated by studying the tangential distribution of intrinsic and inter-areal connections of finger representations of area 1. Retrogradely labeled cell densities and anterogradely labeled fibers and terminal patches were plotted and quantified with respect to the hand representation by combining tract tracing with electrophysiological mapping and intrinsic signal optical imaging in somatosensory areas. Intrinsic connections of distal finger pad representations of area 1 spanned the representation of multiple digits indicating strong cross-digit connectivity. Area 1 distal finger pad regions also established high density connections with homotopic regions of areas 3b and 2. Though similar to area 3b, connections of area 1 distributed more widely and covered a larger somatotopic representation including more proximal parts of the finger representations. The lateral connectivity pattern of area 1 is a suitable anatomical substrate of the emergence of multifinger receptive fields, complex feature selectivity and invariant stimulus properties of the neurons.

For Peer Review

Introduction

Somatosensory cortical area 3b and area 1 represent the initial stages of tactile information processing in primates (Sur et al., 1980; Iwamura, 1998). Both areas are characterized by an orderly, somatotopic representation of the body surface with a disproportionately enlarged hand representation indicating the importance of this region in tactile perception. Despite this common basic somatotopy, areas 3b and 1 exhibit distinct structural and functional organizational features. In contrast to the small receptive fields of area 3b neurons which are confined to single digit tips, the classical receptive fields of area 1 neurons typically span more than one digit (Mountcastle and Powell, 1959; Hyvarinen and Poranen, 1978; Costanzo and Gardner, 1980; Iwamura et al., 1983a, 1993; Sur et al., 1980, 1982, 1985; Sripati et al., 2006; Hsiao, 2008). Compared to area 3b the larger size also represent evolving complexities of the receptive field properties as indicated by the greater intra- and inter-digit integration, larger motion and direction selectivity and feature invariant response properties (e.g. Iwamura et al., 1983b; Iwamura 1998; Sinclair and Burton, 1991; Sripati et al., 2006; Bensmaia et al., 2008; Pei et al., 2010). Lesion of area 3b silences area 1 to peripheral stimulation; conversely, area 3b remains responsive for cutaneous stimulation following area 1 lesions (Garraghty et al., 1990). Anatomical studies show that, compared to area 3b, thalamic input to area 1 is weaker and the majority of input to area 1 originates in area 3b (Jones et al. 1978; Vogt and Pandya 1978; Shanks et al. 1985). All these findings suggest that response properties of area 1 neurons are mostly determined by converging input from area 3b.

The anatomical circuitry underlying the emergent response characteristics of area 1 is unknown. Some possible sources include convergent inputs from either the thalamus (Padberg et al., 2009) or within area 3b (Chen et al., 2003; Reed et al., 2010, 2012; Thakur et al., 2012),

For Peer Review

and cross-digit interactions within area 1 (Friedman et al., 2008). However, studies of local circuitry within somatosensory cortex are few (Juliano et al., 1990; Burton and Fabri, 1995). Using anatomical tracers, Burton and Fabri (1995) reported intrinsic connectivity between neighboring finger representations in area 1 in the macaque monkey. However, they used relatively large injections which may not have been confined to single digit representations. Moreover, the distribution of transported tracer label relative to digit representations was not mapped functionally. Anterograde and retrograde labeling distributions were constructed based on computational unfolding the cross sections; although the work was carefully conducted, there remain possible distortions introduced by such unfolding procedures, which could lead to significant interpretation errors given inter-digit representation distances of 1 mm or less. Given the paucity of data, additional studies of local intrinsic connections in area 1 are needed.

The goal of the present study is to explore the fine scale organization of intrinsic and inter-areal (with areas 3b, 2 and 3a) connectivity of area 1 and to do so with respect to functionally mapped somatotopy. As the fingers and especially the fingertips play a prominent role in active touch and are defining aspect of primate behavior, we have focused on the digit representation region of somatosensory cortex of the squirrel monkey. The cortex in these monkeys is lissencephalic, negating the need to reconstruct tracer label from unfolded cortex and thereby reducing error. Moreover, several areas can be simultaneously mapped with optical imaging and electrophysiological techniques (Chen et al 2001, 2003; Friedman et al 2004; Negyessy et al 2013). These maps are then used to guide focal injections of tracer into identified single digit tip representations and precisely aligned with transported label permitting accurate reconstruction of label respect to these maps. Using these methods, we report distinct inter- and intra-areal axes of information flow in somatosensory cortex: a prominent cross-digit axis within area 1 and a largely intra-digit axis between area 1 and area

For Peer Review

3b. Comparisons with labeling patterns from digit injections in area 3b (Négyessy et al., 2013) are discussed. Preliminary findings of this study have been published in abstract form (Ashaber et al., 2011).

Materials and methods

For Peer Review

Animal preparation

Two males (Mo, P) and one female (M) adult squirrel monkey (*Saimiri sciureus* weighing 600-800 gm, 2-9 years old) served as experimental subjects. Animal care and surgeries were performed according to NIH (National Institute of Health) regulations and were in compliance with and approved by the Institutional Animal Care and Use Committee of Vanderbilt University. Each animal was sedated with ketamine hydrochloride (10 mg/kg), given atropine (0.05 mg/kg), intubated, placed in a stereotaxic frame, and mechanically ventilated with isoflurane anesthesia (0.9–1.3%). Vital signs (blood oxygen saturation (SpO_2), heart rate, ECG, EEG, ET-CO_2, respiratory pattern, temperature) were monitored throughout the experiment. Body temperature was maintained between 37.0 - 38.5 ^{o}C via a circulating water blanket (Gaymar Industries, Orchard Park, NY, USA) and for hydration lactated ringers (with 2.5% dextrose) was infused intravenously (2 ml/kg/hr). After a craniotomy (centered at AP 6 mm and ML 15 mm) and durotomy, the somatosensory cortex including area 3b and area 1 was exposed and identified by blood vessel landmarks and functional mapping (see below). After tracer injection, to provide time for transport, exposed cortex was covered with artificial dura, the craniotomy was closed by securing the bone flap with bone cement, the skin sutured, and the animal awoken from anesthesia with post-operative pain management. For these

studies repeated craniotomies and durotomies over the same area of cortex were separated by at least 10 days.

Functional mapping

Demarcation of areal borders and digit representations were made as described in Négyessy et al. (2013). Following electrophysiological mapping of the hand and the finger pad representations of areas 3b and 1, intrinsic signal optical imaging (IOS) was used to map the distal finger pad representations of fingers D2-D4. Injections were then made into defined distal finger pad regions of area 1. A short description of functional mapping is given below.

Microelectrode electrophysiological mapping. Using the end of the central sulcus as an anatomical landmark, tungsten microelectrodes were inserted into superficial cortical layers to map the somatosensory cortical areas studied. Number of penetrations used for mapping was 46 in case M, 20 in case Mo and 40 in case P. The responsive skin area of the unit activity was identified by palpating areas on the contralateral hand while listening to an audio amplifier for spike activity. As generally observed in squirrel monkeys, area 3b was found slightly anterior to the central sulcus. Area 3b was identified by single and multiunit response properties having small receptive fields (restricted to a single finger) and brisk responsiveness to light touch. Area 1 was identified based on location, as it is found posterior to area 3b; whereas area 3a is located anterior to area 3b (Chen et al., 2001, Friedman et al., 2004, 2008, Sur et al., 1982). Putative area 2 was identified as the region caudal to distal finger pad representation of area 1, exhibiting sensitivity characteristic of deep receptors and tip-to-tip somatotopic organization with area 1.

Finger Stimulation. For topographical mapping with intrinsic optical imaging digit-specific cortical activity was mapped by stimulating the glabrous skin of the distal, middle, and

For Peer Review

proximal finger pads with vibrotactile indentations (detailed descriptions in Chen et al., 2001, 2003, Friedman et al., 2004). Fingers were secured in plasticine leaving the glabrous surfaces available for tactile stimulation. Finger pads (D2-D4) were stimulated with a Teflon probe (2 mm diameter) mounted on a piezoceramic actuator (Noliac, Kvistgaard, Denmark) that was driven by a Grass 88 stimulator (Grass-Telefactor, West Warwick, RI, USA). The tactilestimulus consisted of a 3 sec train of 8 Hz square wave taps (pulse duration of 30 ms; indentation amplitude of 0.48 mm). During rest or the blank condition, a probe was lightly touching the skin.

Image Acquisition. Images with 630 nm wavelength illumination were acquired through an optical chamber with a CCD camera using either a Redshirt Imaging System running CortiPlex software (Redshirt Imaging, Decatur, GA, USA) or an Imager 3001 system (Optical Imaging Inc., Germantown, NY). With a macroscopic tandem lens combination, the majority of the reflected light is derived from the upper 500 μm of cortex (Ratzlaff and Grinvald 1991). A blood-vessel map, used for landmark purposes, was collected with 570 nm illumination. Tactile stimuli were presented in a randomly interleaved manner in blocks typically consisting of 4 conditions (e.g. proximal, middle, distal sites on a single digit, and a blank no stimulus condition, or distal finger pads of D2, D3, D4, and blank). For each condition, 30-50 trials were collected. Intrinsic image maps were collected at 5 image frames per sec for 4 sec starting 200 msec prior to stimulus onset. Inter-stimulus intervals were between 8-10 sec. Estimates of borders between areas 3a/3b were localized to the rostral edge of the digit tip activations in area 3b, and that between area 3b/1 were roughly centered between the digit activations in area 3b and area 1. These estimates were also guided by electrophysiological maps (see below).

For Peer Review

Image Analysis. As the intrinsic signal time course peaks around 2-3 seconds post-stimulus onset, for each stimulus condition, image frames 6-15 were summed and compared to the pre-stimulus (first frame); this helps to maximize the signal-to-noise ratio. To reduce blood vessel artifact we used blank subtraction (where the 'blank' reference was a 3 second image acquired during no stimulus presentation, Blank condition). To delineate regions of strongest activation, images were low-passed filtered with a 10-pixel (150 μm radius) Gaussian spatial filter. To confirm reliability and consistency of the signal, we evaluated the frame-to-frame temporal development of optical images and compared the similarity of images obtained by summing different blocks of trials (Chen et al., 2001; Friedman et al., 2004).

Tracer Injection and Perfusion

To study connections of the distal finger pads, we injected both anterograde and retrograde tracers in selected digit tip locations. Distal finger pad representations of area 1 localized by IOS and electrophysiology were injected with a 1:1 mixture of 10% BDA (biotinylated dextran amine) 10K (preferentially anterograde) and 10% BDA 3K (preferentially retrograde) (final cc 5% each) (Molecular Probes, Inc. Eugene, OR, USA) in 0.01 M phosphate buffer (PB, pH 7.4). Injections were made via iontophoresis (3 μA, 5 seconds on/off cycle) for 2 x 10 minutes at two depths, 750 and 350 μm below the cortical surface. Injections in area 1 were made into the representation of the glabrous skin of the tip of digit 2 (D2t; M, P) and digit 4 (D4t, Mo) exhibiting slowly adapting responses to pressure stimuli. Table 1 summarizes the parameters of the injections for each case, including the physical parameters of the glass micropipettes.

After 10-16 days survival period (M: 14 days, Mo: 16 days, P: 10 days), animals were deeply anesthetized before perfusing transcardially with 300 ml of 0.9 % NaCl in distilled

For Peer Review

water and 1000 ml fixative consisted of 4% paraformaldehyde, 0.1% glutaraldehyde and 0.2% picric acid in 0.1M PB (pH 7.3). Brains were immediately removed and the region of interest was then cut from the cortex, flattened and postfixed overnight.

Tissue processing

Series of 50 µm thick horizontal sections were cut with a vibratome and collected at 160 µm (M, Mo) and 150 µm (P) spacing after cutting 3 x 100 µm thick sections from the very top of the flattened cortex. Among these 3 topmost sections the 1st and 2nd were cut from the arachnoidal tissue and the 3rd included the very surface of neural tissue where the pattern of blood vessels running parallel to the cortical surface were similar in appearance to the previous 2 sections. These thick sections were used for alignment (see below).

The standard ABC protocol (Elite kit, Vector Laboratories, Inc. Burlingame, CA, USA) was used to visualize BDA labeling with nickel intensified diaminobenzidin (NiDAB) (Sigma-Aldrich Kft, Budapest, Hungary) as the chromogen (for more details about the procedure see Négyessy et al., 2000, 2013). In short, sections were incubated with the avidin/biotinylated enzyme complex (ABC, 1:200 in PB, 0.1M, pH 7.4) overnight at 4 ^{o}C after freeze-thawing of the cryoprotected sections (30% sucrose in PB). Unbound aldehydes were reduced by borohydride (1% $NaBH_4$ in PB, 30 min) and intrinsic peroxidase activity was blocked by 1% H_2O_2 in PB (30 min) before the ABC step. Afterwards the NiDAB reaction sections were osmicated (1% OsO_4 (Electron Microscopy Sciences, Hatfield, PA, USA) with 5% sucrose in PB, pH 7.4 for 60 minutes) and flat embedded in resin (Durcupan, Sigma-Aldrich Kft, Budapest, Hungary).

For Peer Review

Data analysis

Data were analyzed in the same way as described in Négyessy et al. (2013). Mapping of the BDA labeling was made with Neurolucida (MicroBrightField Europe, E.K. Magdeburg, Germany) using an Olympus research microscope equipped with a motorized stage (MultiControl 2000, Märzhäuser Wetzlar GmbH & Co. KG, Wetzlar, Germany). Retrograde labeling was mapped at 10x and 20x (objective magnification) while axonal fibers (anterograde labeling) were examined and reconstructed with 20x and 40x objectives. Terminal patches were examined at 10x and 20x and outlined individually on each section. The size of the patches was measured by Neurolucida Explorer using the Feret maximum and Feret minimum functions (Négyessy and Goldman-Rakic, 2005; Négyessy et al. 2013). The average of the Feret maximum and minimum was calculated for comparative analysis. Neurolucida-drawings were edited in Neurolucida Explorer (MicroBrightField Europe, E.K. Magdeburg, Germany). Photomicrographs were taken by a digital camera and edited in Photoshop (Adobe Systems Inc., USA) together with the images exported from the Neurolucida Explorer.

Density plots of the retrograde labeling were generated by way of Voronoi tessellation of two dimensional maps. For a set of points (labeled neurons) this procedure divides a region into polygons where each point in the polygon is closer to the seed point (labeled neuron) than any other seed; neuronal cell densities are then calculated based on the areas of these polygons. The distance between the serial sections was ignored and the reconstructed labeling was projected into a single plane (for more details see Negyessy et al., 2013). The logarithms of Voronoi areas were averaged and the standard deviation (SD) computed to represent deviation from the mean. Target specificity of the injected cortical loci was examined by localizing terminal arborizations of the anterograde labeling. Also, the core of the injection site of 250-300 μm diameter was omitted from the analyses.

For Peer Review

Densities of axon terminal-like structures were sampled with a 100x objective, using Neurolucida in the full depth of each section of the series in 3 neighboring 50 μm^2 frames centered in 3 defined regions which included: 1) terminal patches (P), 2) tracks of long range axons (F) and 3) regions lacking retrograde labeling outside of the previous two areas (CF). Selected regions were localized to areas including areas 3b, 3a, 1 and/or 2. Altogether in the three monkeys 3712 bouton-like structures were counted in 37 regions (19 terminal patches, 14 fibers of passage, 4 without retrograde labeling outside of the previous two). The average and standard deviation computed from the three sampling frames across cases were used to compare bouton densities in the different regions and cortical areas.

Alignment

Sections were scanned with in-house written software with a 4x objective on the microscope used for the Neurolucida reconstruction. In Photoshop, the three topmost sections were aligned with an image of the cortical surface vasculature obtained during optical imaging. The scanned images of the consecutive sections of the 50 μm thick series were then aligned with the topmost sections and to each other by using blood vessel patterns and cut edges of the sections (Figs. 2, 5). Reconstruction of the BDA labeled structures was made using the serial section reconstruction function of Neurolucida, which results in a completely aligned series of the drawings. Finally, the Neurolucida drawings were aligned with their corresponding scanned sections which resulted in the alignment of the serial reconstruction with the cortical surface. For more details see Négyessy et al. (2013).

For Peer Review

Results

In the first part we describe the mapping of the hand representation, the size and localization of the BDA injections and the nature and overall distribution of the labeling. In the second part the pattern of horizontal connectivity is defined on the basis of the somatotopic maps within area 1 and in neighboring areas 3b, 2 and 3a.

For Peer Review

Functional mapping and BDA injections

Electrophysiological and IOS maps. Digit representations of areas 3b and 1 were mapped by IOS and electrophysiological recording in each case as described previously (Negyessy et al., 2013). Extracellular recording of neuronal responses evoked by mechanical stimulation was used to identify the gross topography of the hand representations of areas 3b and 1 (Fig. 1A). Based on known organization of the somatotopic maps (Sur et al. 1982; Kaas, 1983), this procedure was also used to define the borders between the areas of the somatosensory cortex via mapping the rostro-caudal shift of cortical activations accompanying distal-to-proximal digit stimulations (Fig. 1A). The lateral-to-medial cortical representation of the fingers was also determined by IOS following vibrotactile stimulations of the distal finger pads (Fig. 1B-D). The IOS and the electrophysiological maps were in good alignment (Figs. 1, 2). Areal identity was defined on the basis of the response selectivity: receptive fields in areas 3b and 1 exhibited clear topographic progression and had brisk sustained or phasic responses to tactile stimulation. A primary difference between areas 3b and 1 was receptive field size: receptive fields of units recorded in area 3b were small and confined to single digits while those in area 1 were larger, at times spanning 2 or 3 digits (cf. Friedman et al., 2008). The border region between areas 3b and 1 comprised a greater number of sites with palmar receptive fields while

those at the area 3b/3a border were largely located on digit tips (D2t, D3t and D4t) (Figs. 1A, 2A-C). Units in area 3a were difficult to drive with tactile stimulation and were often activated only by sustained, deep stimulation and joint movement, consistent with deep receptor activation previously described for area 3a (Huffman and Krubitzer, 2001; Krubitzer et al., 2004). Some units in area 3a were also activated by thermal stimulation as previously described (Tommerdahl et al., 1996). The border between area 1 and area 2 was often difficult to place with confidence. We typically found units in area 2 had large receptive fields (e.g. some spanning D2 base/join, D3 palm/deep, D2 palm cutaneous), were noticeably more difficult to drive, had more mixed responses (e.g. some heat responses, some deep responses), and were characterized by palmar receptive fields. Thus, we were reasonably confident about the borders between areas 3a and 3b as well as between areas 3b and 1, and less certain about the borders between area 1 and area 2 and between areas 3a and presumed Brodmann area 4 (M1). Injections were then placed iontophoretically at selected sites in area 1 (Figs. 1, 2A-C).

Injection site. The core of the BDA injection sites exhibited dense and diffuse NiDAB labeling, spread through multiple layers and had a diameter of 300-400 μm (Table 1, Fig. 2D-F). A halo of labeling surrounding the core was characterized by a dense plexus of neuronal processes, and was clearly visible in Mo (Fig. 2E). In cases M and P the injection site was more homogenous with a less distinct halo around the core and were considered as the core of the BDA injection (Fig. 2D, F). Within the core, BDA labeling of the perikarya can result from direct uptake of the tracer without retrograde transport, therefore these labeled cell bodies were omitted from the analyses. Based on the electrophysiological recordings, injection was localized within the distal finger pad representation of D4 in case Mo (Fig. 2B). In cases M and P the injections apparently included the representations of the neighboring D1 tip and D2 middle phalange, respectively, in addition to the targeted D2 tip region (Fig. 2A,

For Peer Review

C). Although in Mo and P the injections were on the edge or offset relative to the IOS maps of the stimulated skin location, the size of the injection was similar or smaller than the size of the activated cortical area in all three cases (Fig. 2G-I). This was clearly shown in case M, where the BDA injection targeted just a sub-region of the stimulated distal finger pad (Fig. 2A, G). The vertical spread of the core of the injections is shown in Table 1 (range of Core depth values in Table 1). The core of the injections included the supragranular layers in all three cases and infragranular layers in cases Mo and P.

Characterization of the BDA labeling

Retrograde and anterograde labeling. Input and output connections of the injected locus of area 1 were labeled by retrograde and anterograde BDA transport, respectively, in each case. Both retrograde and anterograde labeling revealed the fine details of the neuronal elements (Fig. 3, 4). The majority of labeled neurons were identified as pyramidal cells bearing frequently branching dendrites decorated by numerous spines and the occasional appearance of the apical dendrite (Fig. 3). Although, a few smooth dendritic neurons were found near to the injection site, these neurons were not specifically considered for further analyses.

Anterograde axonal labeling also revealed the fine branching pattern and the presence of axon terminal like structures including bouton-like structures with stalk and en passant enlargements (varicosities) (Fig. 4C). The anterogradely labeled fibers could be divided into three types: 1, terminal-like patches formed by a dense network of thin fibers with several bouton-like enlargements in a circumscribed cortical localization (Fig. 4 A-C) 2, relatively thick, horizontally oriented long fibers decorated by bouton-like structures (Fig. 4D) and 3, smooth, long range fibers lacking bouton-like structures (Fig. 4D).

For Peer Review

Terminal axon arborizations. Patches formed by terminal axon arborizations are likely to be localized at preferred target areas of the injected cortical sites. After outlining we quantified the patch size (see methods) and compared the density of bouton-like structures within and outside of the patches (Fig. 5). Average patch diameters were about 350 μm (Fig. 5D). Average patch size did not significantly differ between cases and areas as shown by two-way repeated measures ANOVA.

If terminal patches are regions of synaptic integration, then we predicted there would be greater percentage of boutons within patch zones than outside patch zones. We therefore quantified the density of axon terminal-like structures in three types of locations: regions containing patches of terminal like axon arborizations (P), regions containing fiber tracts (F), and regions devoid of BDA cell bodies and labeled axonal tracts (CF) (Fig. 5A-C). Figure 5E shows the mean of the ratio and standard deviation of bouton-like structures in each of these three regions after combining the data from the individual cases. Regions containing patches of terminal like axon arborizations (P) had a several fold higher density of bouton-like structures than regions containing only fiber tracts (F) or devoid of labeled fiber bundles or cell bodies (CF). Accordingly, comparing ratios of the bouton-like structures of the three regions (P, F, CF) using a one-way ANOVA indicated significant differences ($p=0.01$). Post hoc comparison showed significant differences between P as compared to F and CF (Fisher LSD test, $p=0.03$ and 0.004, respectively). The density of bouton-like structures between F and CF was not statistically different. This result supports the notion that terminal arbors are likely to be regions of greater synaptic integration.

Distribution of retrograde and anterograde labeling

For Peer Review

In this section we first describe the patterns of retrograde and anterograde labeling resulting from area 1 digit tip injections. Then we discuss the relationship to mapped digit topography.

Retrograde labeling

The Voronoi diagram affords a measure of the retrograde labeling density at the neuronal level, therefore binning was not necessary. By avoiding binning, the Voronoi density map provides an undistorted, topographically appropriate and high resolution density distribution. Because the size of the Voronoi polygons is determined by the distance of the retrogradely labeled neurons from the neighbors or seeds, the smaller polygon indicates higher densities and vice versa. As the size of the polygons is a largely varying, continuous variable a simple color coding became necessary to illustrate major connectional density gradients. For this purpose the deviation of the size of the area of the Voronoi polygons from the mean was computed and colored by dividing the deviations into ranges of unit sizes of standard deviation.

We observed two major patterns of retrograde labeling within and across cortical areas in the two dimensional reconstructions (Fig. 6A-C). Within area 1, in all three cases, the highest density of labeling appeared around the injection sites and the density of labeling decreased and became scattered further away. The size of this strongly labeled region varied; it was similar in cases M and Mo and exhibited the largest extent in case P (Fig. 6A-C). Computation of the density maps compensated for individual differences and made the pattern of retrograde labeling more comparable across cases (Fig. 7): note within area 1 the extent of the color coded regions marked by yellow and green on the SD maps (Fig. 7). Around the injections site the yellow region representing a density 1 SD above the average occupied a region of roughly 1 mm of diameter in the three cases within area 1 (Fig. 7). The density maps

For Peer Review

also show the gradual decrease of the retrograde labeling away from the injection sites in area 1 (Fig. 7).

Following single digit tip injections in area 1, patterns of labeled cell clusters was observed in neighboring somatosensory cortical areas (Figs. 6A-C, 7). In each animal high density retrograde labeling was found within a relatively small, circumscribed region of area 3b (Fig. 7). This region is very clearly outlined on the density maps in cases M and Mo (yellow and green areas on Fig. 7A, B). In case P the clustering of the retrograde labeling was more apparent in the raw data (Fig. 6C) since the average density in area 3b did not reach above +1 SD (yellow) due probably to the very high density labeling near the injection site (Fig. 7). Instead, closely spaced fragments of near average density regions (green regions representing -1 SD) were found (Fig. 7C). In general, the area of high density labeling was smaller in area 3b than in area 1 in all the cases (Fig. 7). In addition, in area 2 another cluster of retrogradely labeled neurons emerged in case P and to a somewhat less extent in case M (Figs. 6A, C; 7A, C). Notably, the density analyses showed that labeling in area 2 also tended to be clustered in case Mo (Fig. 7B). The pattern of clustering in area 2 was less obvious than in area 3b and 1 perhaps because only part of this area was preserved. The relatively high density labeling across the border between area 1 and 2 could represent the tip-to-tip organization of the hand representation of these two areas (Fig. 7).

Anterograde labeling

A massive bundle of anterogradely labeled, long range fibers were observed rostral from the injection site entering area 3b and passing even further to area 3a and probably to motor cortical area 4 (M1) in Mo and P (marked by blue on Fig. 6E, F). Similarly, a dense, BDA labeled axonal pathway was directed caudally from the injection into area 2 of Mo and P (shown by green on Fig. 6E, F). This caudal plexus of the BDA labeled axons was

For Peer Review

apparently shorter than the one moving into the rostral direction. An additional course of fibers was oriented mediolaterally and restricted mostly to area 1, therefore representing mostly long range intrinsic connections (red lines in Fig. 6E, F). In case M, only short segments of the horizontally running fibers could be reconstructed because of the oblique cut of the sections (Fig. 6D).

Terminal patches of axon arborizations were widely distributed with biases in the mediolateral orientation within area 1, while in area 3b a more focused distributional pattern was found (black contours on Fig. 6D-F). Case P was an exception by having a similarly widespread mediolateral distribution of the terminal patches both in areas 1 and 3b (Fig. 6F). Within area 1 patches grouped closer to the caudal border (Fig. 6D-F). Although, in area 3b the terminal patches apparently distributed more evenly in the rostrocaudal direction, a higher overlap tended to be localized closer to the anterior border of the area in the three cases (Fig. 6D-F). Terminal patches also accumulated in areas 3a and caudal to area 1, most probably within area 2, where the distribution of patches was spatially restricted (Fig. 6D-F). Case P was an exception, where patches spread rostrocaudally in presumed area 2 (Fig. 6F). Laterally placed patches were also observed in presumed area 2 of case Mo (Fig. 6E). In all cases terminal axon arborizations distributed along the BDA labeled fiber bundles (Fig. 6D-F).

For Peer Review

Reciprocity

It is important to note that reciprocal connectivity was studied between somatotopically identified cortical regions on the 2D maps. It is possible, that while anterograde and retrograde labeling overlapped on the horizontal maps i.e. identified reciprocal, their laminar distribution could have been distinct. Laminar distribution was not

examined in this study. Also, our data can not reveal direct reciprocal connections between neuronal cells.

The overlapping distribution of retrograde and anterograde labeling indicated a reciprocal organization of area 1 connectivity (Figs. 6, 7). Reciprocity appeared as an overlap of the terminal patches of axon arborizations with the regions exhibiting local peaks of density of the retrogradely labeled neurons (Fig. 7A-C). The findings suggest that connections of the distal finger pad regions of area 1 are organized preferentially in a reciprocal way at the regional level. One major exception was area 3a, where dense terminal axon arborization colocalized with a low density retrograde labeling in Mo and P (Fig. 7B, C). Another exception, which was especially prominent in case Mo (Fig. 7B), appeared laterally in presumed area 2 near the area 1 border, where terminal patches did not align with peaks of retrograde labeling densities. Although, unreciprocated connections could be a result of section sampling, further studies are needed on a complete series of sections to unequivocally resolve the question of regional reciprocity of the input and target connections of area 1.

For Peer Review

Input and target specificity of the distal finger pad representations of area 1

Input preference – Retrograde labeling

With respect to the intrinsic cortical circuitry of area 1, the highest density of retrograde labeling occupied either fully (case M) or in a large part (cases Mo and P) the injected distal finger pad representation, based on the combined electrophysiological and IOS maps (yellow and orange on Fig. 8 A-C). In all three cases the high density region marked by the extent of the green area was elongated rostrally suggesting considerable input from the representation of the proximal finger to the injected digit tip representation (Fig. 8A-C). This

localization pattern was evident on the detailed electrophysiological maps (Fig. 7). In case M e.g. the high density input region colocalized with the representation of the proximal part of D2 (yellow in d2p on Figs. 7A; 8A). Similarly, in P the stimulation of the mid phalanx of D2 evoked neuronal activity in a region with high density retrograde labeling (d2m on Fig. 7C). High density input to the injected digit representation also originated from neighboring finger representations. Accordingly, injection of the D4t representation resulted in high density labeling in the D3t region in case Mo (green and yellow in Fig. 8B). However, labeling density dropped to a low level in the non-neighboring finger representations in this case (blue and pink on Fig. 8B). Similar observations were made in case M, where injection of the D2t representation resulted in low density retrograde labeling in the D4t region (blue in Fig. 8A) while the neighboring D3t and also the D1t representations were densely labeled (yellow and green on Fig. 8A). In case P injection of the D2t representation resulted in lateral high density labeling in the D1t representation (Fig. 7C). Medially, the D3t region identified electrophysiologically included high density retrograde labeling, whereas further medially within the D3t region identified by IOS labeling density dropped to a low level (Fig. 8C). This case also exhibited widespread connections originating from more the proximal finger representations to the injected fingertip location (Figs. 7C, 8C).

Inter-areal connections with area 3b were characterized by the appearance of a high density cluster indicating that the major input to the injected fingertip region of area 1 originated from the homotopic finger representation region (Fig. 8A-C). This pattern was clearly seen in cases M and Mo (overlap of yellow and orange with the D2t and D4t representations, respectively on Fig. 8A, B). In case P, the highest density retrograde labeling of area 3b was localized not only in the homotopic D2t region but also laterally within the D1t representation (green areas on Fig. 8C). Similarly, a relatively high density spot appeared within the presumed D1 representation in the vicinity of the d1m responsive area of case M

For Peer Review

(green region at d1m in Fig. 8A). Interestingly, in cases M and P medial to the D2t region, retrograde labeling density decreased to a low level in the D3t representation (blue and pink on Figs. 7A, C, 8A, C). An asymmetric, laterally skewed distribution also appeared in case Mo, where following the injection of the D4t region of area 1, a relatively high density retrograde labeling was found in the D3t region (blue on Fig. 8B), while labeling density substantially decreased medially to the D4t region representing presumably D5 in area 3b (pink on Figs. 7B, 8B). Notably, a relatively high density retrograde labeling spread caudally in area 3b into regions representing presumably the proximal parts of finger D2 in cases M and P and of D4 in case Mo in area 3b (Figs. 7, 8A-C).

High density labeling was also localized caudally in presumed area 2 next to the injected finger pad representation, which suggest a similar homotopic topography of the inter-areal input from this region to area 1 (rostrocaudal spread of the green and blue region in area 3b on Fig. 7,).

Target preference – Anterograde labeling

Within area 1 the D2t representation gave birth to terminal axon arborizations localized nearby the injection site within the D2t region (Fig. 8D, F). Additional terminal patches were localized anterior to the injection targeting presumably the representation of the more proximal parts of D2 or the neighboring fingers (Fig. 8D, F). Considerable lateral spread of terminal axon arborizations was found in case P, where patches were localized laterally in a region representing presumably D1, based on the localization of D1 in area 3b of this case (Fig. 8F). Similar to the retrograde labeling, case P also exhibited a large divergence of labeled afferents with terminal arborizations located in regions presumably representing proximal parts of the different fingers (Fig. 8F). In case Mo, injection of the D4t

For Peer Review

representation resulted in the labeling of terminal axon arborizations lateral to the injection site within the representations of D3t and D2t (Fig. 8E).

In area 3b terminal patches densely accumulated in the homotopic distal finger pad representations, i.e. within the D2t region of cases M and P and in D4t region of case Mo (Fig. 8D-F). In cases Mo and P terminal patches were also found laterally in the neighboring D3t and D1t regions, respectively (Fig. 8E, F). Case P also included the labeling of terminal patches in areas medial to the D2t representation, which could represent neighboring D3 and/or D4 (Fig. 8F).

Other inter-areal target sites included area 2 where numerous terminal patches close the estimated area 1/2 border in the vicinity of the injected distal finger pad representations suggested similar homotopic topography of patch distribution as in the case of the retrograde labeling (Fig. 8D-F). Some terminal patches also appeared laterally (all three cases) and also medially (cases Mo and P) from the above mentioned region, which suggest some divergence of the afferents of the distal finger pad regions within the cortical area caudal to area 1 (Fig. 8D-F). In case Mo, dense accumulation of terminal patches was localized caudolateral to the D4t injection, which might be the region of area 2 representing neighboring D3t on the basis of the topography found in area 1 (Fig. 8E). Within area 3a in cases Mo and P terminal patches were clustered within a circumscribed region in the vicinity of the homotopic finger representation of area 3b suggesting a similar homotopic topography of terminal patch distribution in area 3a as well (Fig. 8E, F).

For Peer Review

Discussion

Our combined anatomical, optical imaging and electrophysiological studies demonstrate that intrinsic connections of area 1 connect neighboring distal finger pad representations in the non-human primate, clearly extending beyond single digit somatotopic activations (Friedman et al 2009). In contrast, inter-areal connections of distal finger pad regions of area 1 establish high density connections largely with homotopic regions of areas 3b and 2. Furthermore, both intrinsic and inter-areal connections of area 1 distal finger pad regions spread into more proximal representation of the fingers.

General considerations

Consistent with what has been described in macaque area 1 (Burton and Fabri, 1995), horizontal cortical connections exhibit a lateral spread beyond the distal finger pad representations of area 1 of the squirrel monkey. Here, we have identified the extent of the lateral spread of intrinsic and inter-areal connectivity with respect to correlated functional maps. The highest densities of labeling were restricted to the representations of the injected finger and its immediate neighbors, similar to that found after similar injections in area 3b (Négyessy et al., 2013). Compared to the pattern observed in area 3b (Négyessy et al., 2013), the fingertip regions of area 1 are connected more strongly with the proximal parts of the injected finger representations, which is consistent with the physiological observations (Iwamura et al., 1983b). Our observations also show that connections of area 1 finger representations are largely reciprocal on the 2D somatotopic maps (but not at the laminar or cellular levels, which were not studied here). One exception may lie in the connections with area 3a: while area 1 receives only a low density connection from area 3a, it provides relatively high density projection to this area. This finding is in agreement with the results of

For Peer Review

degeneration studies showing that micro-lesions in area 1 result in anterograde but not retrograde degeneration in area 3a (Shanks et al., 1985).

A notable difference found after the area 1 injections in the present study as compared to that of area 3b injections by Négyessy et al. (2013) is that on the retrograde density maps the peak densities were surrounded by a larger spread of medium to low density regions, which together occupied an apparently larger cortical territory than the activated region on the optical imaging maps both in areas 3b and 1. This pattern of cortical connectivity implies that within area 1 high density, digit-matched inputs from area 3b forms the anatomical basis of receptive field hotspots and the lower density flanking regions could provide convergent input from neighboring fingertip representations to form the multi finger receptive fields. Conversely, as shown by the distribution of the terminal axon arborizations, area 1 afferents originating from the distal finger pad could modulate not only the homologous but also the neighboring fingertip representations as well as more proximal representations of the injected fingers in areas 3b. This observation is consistent with a recent study showing that injecting multiple finger representations of area 3b result in overlapping labeling of the different finger representations of area 1 (Liao et al., 2013).

Technical considerations

The major findings were observed in all three cases used in this study. Some differences observed between the cases are discussed below. In case P, BDA injection resulted in a larger amount of retrograde and anterograde labeling and a more widespread distribution of the intrinsic connectivity than in the other two cases. The large mediolateral extent of the labeling in the rostral part of area 1 of case P suggests that intrinsic connections could include proximal parts of the finger representations throughout area 1. In P the injection was offset to the optical imaging map representing the center of the injected finger pad and could have been

For Peer Review

included a region representing a more proximal part of the finger as indicated by the closeness of the middle phalange on the electrophysiological map (Figure 2C). Similarly, in case Mo the injection targeted the periphery of the center of the distal finger pad representation on the IOS map, which could result in a slight shift of the labeling density relative to the IOS activation pattern in area 3b as well. However, the electrophysiological map indicated that the injection site was localized within the distal finger pad representation of area 1 in Mo. Possible pitfalls of bidirectional tracing have been discussed in Négyessy et al. (2013).

Functional speculations

Recent electrophysiological studies have revealed complex spatiotemporal receptive field structures in areas 3b and 1 (Sripati et al., 2006; Reed et al, 2010, 2012; Thakur et al., 2012). These findings are in agreement with the distribution of intrinsic and inter-areal connections of distal finger pad representation of area 1 and area 3b (Négyessy et al., 2013). Accordingly, intrinsic connections were found between neighboring distal fingertip regions and a heavy inter-areal connection was localized to the homotopic representations. However, compared to area 3b, Sripati et al. (2006) observed larger nonlinearities of the area 1 receptive field structure and proposed that such processes could, in part, be responsible for features such as more complex spatial and less velocity selectivity. Compared to area 3b, the larger spread of intrinsic and inter-areal connections of area 1 distal fingertip regions could be an anatomical substrate of such non-linearity. Specifically, surround inhibition, which is increased in area 1 when compared to that in area 3b (Sripati et al., 2006) is thought to be mediated, at least in part, by long range intracortical interactions (Angelucci and Bressloff, 2006; Shushruth et al., 2009). Further possible functional role for intrinsic horizontal connectivity is suggested by Reynaud et al. (2012) showing that in visual cortex V1 lateral cortical interactions compute local input normalization, an important step of contextual modulation. In area 1 such lateral

For Peer Review

cortical interactions could play important role in processing invariant response properties observed in cases of velocity, texture, form, speed and intensity (e.g. Sinclair and Burton, 1991; Pei et al. 2010). In contrast to the intrinsic connections, feed forward input from area 3b may be integrated more linearly in area 1. As shown by Pei et al. (2011) direction selectivity of area 1 neurons arises as vector averages of local motion detectors of area 3b. These findings together raise the question whether selective stimulus properties of area 1 neurons are formed by linear integration of convergent feed forward afferents of area 3b while invariant feature properties are computed by lateral intrinsic and possibly feedback connections from higher order somatosensory areas in area 1. More studies on different feature selective properties are needed to answer this question. While the present findings that connections of area 1 exhibit somewhat larger spatial spread than that of area 3b are consistent with the physiological observations and support the idea of an increasing convergence of intrinsic and inter areal connections of area 1 (Jones, 1975, Iwamura, 1998) more studies at even higher spatial resolution will be necessary to map the circuitries responsible for the functional characteristics of area 1.

For Peer Review

Acknowledgements. The technical assistance of Laura Trice, Tünde Magyar, Yan Yan Chu and Alyssa Zuehl is highly appreciated.

Conflict of interest statement. The authors have no conflict of interest.

Role of authors. Study concept and design: LN, AWR. Acquisition of data: MA, LN, EP, RMF, LMC, BJ, OK. Analysis and interpretation of data: LN, AWR, RMF, MA, CP. Drafting of the manuscript: LN, MA, RMF, AWR. Statistical analysis: LN, MA, CP. Obtained funding: LN, AWR.

For Peer Review

References

Angelucci A, Bressloff PC. 2006. Contribution of feedforward, lateral and feedback connections to the classical receptive field center and extra-classical receptive field surround of primate V1 neurons. Prog Brain Res 154:93-120.

Ashaber M, Palfi E, Palmer C, Friedman R, Chen L, Roe A, Negyessy L. 2011. Preferential connections of area 1 fingertip representation in primary somatosensory cortex of squirrel monkey. 13th Conference of the Hungarian Neuroscience Society (MITT). Front Neurosci doi: 10.3389/conf.fnins.2011.84.00083

Bensmaia SJ, Denchev PV, Dammann JF 3rd, Craig JC, Hsiao SS. 2008. The representation of stimulus orientation in the early stages of somatosensory processing. J Neurosci. 28(3):776-86.

Burton H, Fabri M. 1995. Ipsilateral intracortical connections of physiologically defined cutaneous representations in areas 3b and 1 of macaque monkeys: projections in the vicinity of the central sulcus. J Comp Neurol 355:508-38.

Chen LM, Friedman RM, Ramsden BM, LaMotte RH, ROe AW. 2001. Fine-scale organization of SI (area 3b) in the squirrel monkey revealed with intrinsic optical imaging. J Neurophysiol 86:3011-29.

Chen LM, Friedman RM, Roe AW. 2003. Optical imaging of a tactile illusion in area 3b of the primary somatosensory cortex. Science 302:881-5.

Costanzo RM, Gardner EP. 1980. A quantitative analysis of responses of direction-sensitive neurons in somatosensory cortex of awake monkeys. J Neurophysiol 43**:**1319-41.

DiCarlo JJ, Johnson KO. 1999. Velocity invariance of receptive field structure in somatosensory cortical area 3b of the alert monkey. J Neurosci 19:401-19.

For Peer Review

Friedman RM, Chen LM, Roe AW. 2004. Modality maps within primate somatosensory cortex. Proc Natl Acad Sci USA 24:101:12724-9.

Friedman RM, Chen L, Roe AW. 2008. Responses of Areas 3b and 1 in Anesthetized Squirrel Monkeys to Single- and Dual-Site Stimulation of the Digits. J Neurophysiol 100**:**3185-3196.

Garraghty PE, Florence SL, Kaas JH. 1990. Ablations of areas 3a and 3b of monkey somatosensory cortex abolish cutaneous responsivity in area 1. Brain Res 528:165-9.

Hsiao, S., 2008. Central mechanisms of tactile shape perception. Curr Opin Neurobiol 18:418-24.

Huffman KJ, Krubitzer L. 2001. Area 3a: topographic organization and cortical connections in marmoset monkeys. Cereb Cortex 11:849-867.

Hyvarinen J, Poranen A. 1978. Receptive field integration and submodality convergence in the hand area of the post-central gyrus of the alert monkey. J Physiol 283:539-56.

Iwamura Y, Tanaka M, Sakamoto M, Hikosaka O. 1983a. Functional subdivisions representing different finger regions in area 3 of the first somatosensory cortex of the conscious monkey. Exp Brain Res 51:315-326.

Iwamura Y, Tanaka M, Sakamoto M, Hikosaka O. 1983b. Converging patterns of finger representation and complex response properties of neurons in area 1 of the first somatosensory cortex of the conscious monkey. Exp Brain Res. 51:327–337.

Iwamura Y, Tanaka M, Sakamoto M, Hikosaka O. 1993. Rostrocaudal gradients in the neuronal receptive field complexity in the finger region of the alert monkey's postcentral gyrus. Exp Brain Res 92: 360-8.

Iwamura Y. 1998. Hierarchical somatosensory processing. Current Opinion in Neurobiology 8:522-528.

For Peer Review

Jones EG. 1975. Lamination and differential distribution of thalamic afferents within the sensory-motor cortex of the squirrel monkey. J Comp Neurol 160:167-203.

Jones EG, Coulter JD, Hendry SH. 1978. Intracortical connectivity of architectonic fields in the somatic sensory, motor and parietal cortex of monkeys. J Comp Neurol 181:291-347.

Juliano SL, Friedman DP, Eslin DE. 1990. Corticocortical connections predict patches of stimulus-evoked metabolic activity in monkey somatosensory cortex. J Comp Neurol 298:23-39.

Kaas JH. 1983. What, if anything, is SI? Organization of first somatosensory area of cortex. Physiol Rev 63:206-31.

Krubitzer L, Huffman KJ, Disbrow E, and Recanzone G. 2004. The organization of area 3a in macaque monkeys. J Comp Neurol 471:97-111.

Liao CC, Gharbawie OA, Qi H, Kaas JH. 2013. Cortical connections to single digit representations in area 3b of somatosensory cortex in squirrel monkeys and prosimian galagos. J Comp Neurol (in press)

Mountcastle VB, Powell TP. 1959. Central nervous mechanisms subserving position sense and kinesthesis. Bull Johns Hopkins Hosp 105:173-200.

Négyessy L, Gál V, Farkas T, Toldi J. 2000. Cross-modal plasticity of the corticothalamic circuits in rats enucleated on the first postnatal day. Eur J Neurosci 12:1654-1668.

Négyessy L, Goldman-Rakic PS. 2005. Subcellular localization of the dopamine D2 receptor and coexistence with the calcium-binding protein neuronalcalcium sensor-1 in the primate prefrontal cortex. J Comp Neurol 488:464-75.

Négyessy L, Pálfi E, Ashaber M, Palmer C, Jákli B, Friedman R M, Chen L M, Roe A W. 2013. Intrinsic horizontal connections process global tactile features in the

For Peer Review

primarysomatosensory cortex: Neuroanatomical evidence. J Comp Neurol. 521:2798-2817.

Padberg J, Cerkevich C, Engle J, Rajan A T, Recanzone G, Kaas J, Krubitzer L. 2009. Thalamocortical connections of parietal somatosensory cortical fields in macaque monkeys are highly divergent and convergent. Cereb Cortex 19:2038-64.

Pei YC, Denchev P V, Hsiao SS, Craig JC, Bensmaia SJ. 2009. Convergence of submodality-specific input onto neurons in primary somatosensory cortex. J Neurophysiol 102:1843-53.

Pei YC, Hsiao SS, Craig JC, Bensmaia SJ. 2010. Shape invariant coding of motion direction in somatosensory cortex. PLoS Biol 8:e1000305.

Pei YC, Hsiao SS, Craig JC, Bensmaia SJ. 2011. Neural mechanisms of tactile motion integration in somatosensory cortex. Neuron 69:536-547.

Qi HX, Chen LM, Kaas JH. 2011. Reorganization of Somatosensory Cortical Areas 3b and 1 after Unilateral Section of Dorsal Columns of the Spinal Cord in Squirrel Monkeys. J Neurosci 31:13662-13675.

Ratzlaff EH, Grinvald A. 1991. A tandem.lens epifluorescence macroscope: hundred-fold brightness advantage for wide-field imaging. J Neurosci Methods 36:127-37.

Reed JL, Pouget P, Qi HX, Zhou Z, Bernard MR, Burish MJ, Kaas JH. 2012. Effects of spatiotemporal stimulus properties on spike timing correlations in owl monkey primary somatosensory cortex. J Neurophysiol 108:3353-3369.

Reed JL, Qi HX, Pouget P, Burish MJ, Bonds AB, Kaas JH. 2010. Modular processing in the hand representation of primate primary somatosensory cortex coexists with widespread activation. J Neurophysiol 104:3136-3145.

For Peer Review

Reynaud A, Masson GS, Chavane F. 2012. Dynamics of local input normalization result from balanced short- and long-range intracortical interactions in area V1. J Neurosci 32: 12558-69.

Shanks MF, Pearson RC, Powell TP. 1985. The ipsilateral cortico-cortical connexions between the cytoarchitectonic subdivisions of the primary somatic sensory cortex in the monkey. Brain Res 356:67-88.

Shushruth S, Ichida JM, Levitt JB, Angelucci A. 2009. Comparison of Spatial Summation Properties of Neurons in Macaque V1 and V2. JNeurophysiol 102**,** 2069-2083.

Sinclair RJ, Burton H. 1991. Neuronal activity in the primary somatosensory cortex in monkeys (Macaca mulatta) during active touch of textured surface gratings: responses to groove width, applied force, and velocity of motion. J Neurophysiol 66:153-169.

Sripati AP, Yoshioka T, Denchev P, Hsiao SS, Johnson KO. 2006. Spatiotemporal receptive fields of peripheral afferents and cortical area 3b and 1 neurons in the primate somatosensory system. J Neurosci 26:2101-14.

Sur M, Merzenich MM, Kaas JH. 1980. Magnification, receptive-field area, and hypercolumn size in area-3b and area-1 of somatosensory cortex in owl monkeys. J Neurophysiol 44:295-311.

Sur M, Nelson RJ, Kaas JH. 1982. Representations of the body surface in cortical areas 3b and 1 of squirrel monkeys: comparisons with other primates. J Comp Neurol 211**:**177-92.

Sur M, Garraghty PE, Bruce CJ. 1985. Somatosensory cortex in macaque monkeys: laminar differences in receptive field size in areas 3b and 1. Brain Res 342:391-5.

Thakur PH, Fitzgerald PJ, Hsiao SS. 2012. Second-order receptive fields reveal multidigit interactions in area 3b of the macaque monkey. J Neurophysiol 108:243-62.

For Peer Review

Tommerdahl M, Delemos KA, Vierck CJ Jr, Favorov OV, Whitsel BL. 1996. Anterior parietal cortical response to tactile and skin-heating stimuli applied to the same skin site. J Neurophysiol 75:2662-2770.

Vogt BA, Pandya DN. 1978. Cortico-cortical connections of somatic sensory cortex (areas 3, 1 and 2) in the rhesus monkey. J Comp Neurol 177:179-191.

For Peer Review

Table 1. Characteristics of the BDA injections in the three cases M, Mo and P. Values are given in μm. Size of the glass capillary measured after the injection is shown. Tip diameter represents the inner diameter of the glass capillary used for the BDA injection. Injection depth was measured from the pial surface by a micromanipulator. Core diameter was measured in the series of the sections where it exhibited the densest and the largest extent. Core depth: approximate depth of the densest and the largest core diameter in the section series. Difference between the injection and core depths could result by pulsation and swelling of the brain during the injection. In Mo, core depth exhibited a bilaminar pattern as the core diameter was smaller at 640 μm than on the neighboring upper and lower sections in the series at 320 and 800 μm, respectively.

	Tip diameter	Injection depth	Core diameter	Core depth	Number of slides	Depth of granular layer
M	30	350, 750	313	320	9	480
Mo	10	350, 750	295	160-800	16	640
P	10	350, 750	403	160-800	10	650

For Peer Review

Figure legends

Figure 1. Mapping the glabrous part of digit representations in the somatosensory cortex with electrophysiology and optical imaging (Case M is shown). (A) Colored dots indicate electrophysiological recording sites. White ellipsoids encapsulate functional regions of similar somatotopic response preference shown also by the same color of the dots. d1-d5: digits 1-5; d1t-d5t: digit tips of fingers 1-5; d2m-d4m: middle phalanges of fingers; 2-4; d2p: proximal paert of finger 2; p: palm. The localization of BDA injection is indicated by the asterisk in the d2t region of area 1. (B) Optical image of the somatosensory cortex without stimulations. (C, D) Optical images the response of somatosensory cortex to stimulation of the D2 (C) and D4 (D) distal finger pads. Red arrows show corresponding vessel landmarks on the different images. Note the medial shift of D4 activation relative to the D2 activation sites in areas 3b and 1. Dashed lines: extrapolated borders between the areas. r: rostral, m: medial, scale bar represents 1 mm.

Figure 2. Localization and size of the BDA injection is shown on maps which include the electrophysiological and intrinsic optical signal (IOS) functional maps of somatosensory cortex in the three cases (M, Mo, P). (A-C) Overview of the cortical surface mapped by electrophysiology and IOS. Black outlines encircle the representation of the distal finger pad regions localized by IOS for the 3 cases. Dotted lines represent areal borders. Electrophysiological recording sites are marked by different symbols shown in the inset. (D-F) Bright field photomicrographs of the injection sites taken from the supragranular layers at a depth of 320 μm (M, Mo) and 450 μm (P) from the cortical surface. Note the core and halo

For Peer Review

organization of the BDA injection sites, which is best seen in Mo. Inner white spotted circle indicates the extent of the core, and the external circle shows the margin of the halo organization of the BDA injection. Core and halo regions could not be clearly delineated in M and P, where the highest density regions were encircled. The black holes represent cross sections of descending blood vessels (asterisk). Arrows point on BDA labeled neuronal cell bodies. (G-I) Higher magnification shows the size of the BDA injection relative to the size of the cortical area activated in the IOS experiments in the three cases. Dark field like views, where image brightness was inverted, are shown to enhance visibility. Small circle with white core: BDA injection sites; Scale bar on A represent 1 mm also applies to B and C; scale bar on D and G represent 250 μm applies also to E, F and H, I, respectively.

Figure 3. Retrogradely labeled neurons. (A) Pyramidal cells as identified by the appearance of the apical dendrites down the focal depth. White arrows indicate cross sections of the apical dendrites. Arrowhead: a horizontal branch originating from the apical dendrite with a protrusion. (B) A pyramidal neuron can be seen in the vicinity of the injection site (dark area in the bottom). Asterisk indicates an electrode track made during the electrophysiological mapping. Framed region is enlarged in the inset showing dendritic spines (arrowhead). Note thin, varicose axonal fiber bending around a blood vessel cut across (white "hole"). (C) Pyramidal cell with widely branching basal dendrites in the supragranular layer. Spiny dendritic spines (black arrowheads) and protrusions (white arrowheads) appear on higher magnification of the framed region in the inset. Scale bars represent 100 μm on (A), 50 μm on (B, C) and 25 μm in the inset.

Figure 4. Anterograde labeling. (A) *Pale contour* outlines a terminal patch of axonal arborizations. Note the low number of retrogradely labeled neurons (appearing as black dots) within the patch. The diagonal dark stripe is a chatter of the vibratome sectioning. (B) Dotted

For Peer Review

line shows the border between the patch (lower left) and the neighboring region with low density BDA labeling. (C) Higher magnification reveals the presence of numerous thin fibers decorated by bouton-like structures. Arrowheads show terminal-like ending with stalk, arrow indicates varicosity. Asterisks mark unlabeled neuronal cell bodies partially surrounded by thin axons. (D) Long range horizontal axonal fibers with (black arrows) and without (white arrows) bouton-like varicosities (black and white arrows, respectively). Note the thick and smooth appearance of the fiber shown by the white arrow. Scale bars represent 250 μm on (A), 50 μm on (B, D) and 25 μm on (C).

Figure 5. Size of terminal patches and density of bouton-like structures. (A-C) Overall distribution of the regions sampled for bouton density analysis on the two-dimensional reconstructions of the retrograde and anterograde labeling in M, Mo and P. Fibers are indicated by light gray curves and patches are marked by circular outlines. Black dots: retrogradely labeled neurons. CF: cell free region, F: fiber tracts and P: terminal patches. (D) Average patch size in the different cortical areas (1, 3b, 3a and 2). (E) The ratio (relative to the total counts in each case) of the average number of bouton-like structures is shown within the three different sampled regions (CF, F, P). Asterisk marks significant difference both from CF and F regions. Error bars indicate standard deviations. Scale bar represents 1 mm.

Figure 6. Retrograde and anterograde labeling in the three cases (M, Mo and P). (A-C) Distribution of retrograde labeling. Green triangles: retrogradely labeled neurons. Injection sites are marked by red dots. (D-F) Distributions of the anterograde labeling. Black outlines show terminal axon arborizations. Red lines: intrinsic connections, green lines: connections with area 2 and blue shows connections with areas 3b and 3a and perhaps M1. Red dotted lines represent areal borders. CS: central sulcus. Scale bars represent 1 mm. r: rostral, m: medial.

For Peer Review

Figure 7. Alignment of the distribution of the terminal axon arborizations, the retrograde density plots and the functional electrophysiological maps. Color code for retrograde labeling density is given in units of standard deviation (SD) above and below average (for further details please see the Data analysis subsection). Dashed lines represent extrapolated borders between the areas. Colored dots indicate electrophysiological recording sites. White ellipsoids encapsulate functional regions of similar somatotopic response preference. d1-d5: digits 1-5; d1t-d5t: digit tips of fingers 1-5, d2m-d4m: middle phalanges of fingers 1-5*;* p: palm. Large white dots with black outline*:* injection site. White region around the injection site shows the area omitted from the analyses (250-300 μm diameter). r: rostral, m: medial, scale bar represents 1 mm.

Figure 8. Alignments of the structural and functional maps in the three cases. (A-C) Input preference is shown by projecting the electrophysiological (pale outlines) and intrinsic optical signal (black outlines) maps on the 2 dimensional density plots of the retrograde labeling. (D-F) Target preference is defined by aligning the terminal patches (red outlines) with the functional maps. Conventions are the same as in Figure 7. Scale bar represents 1 mm.

For Peer Review

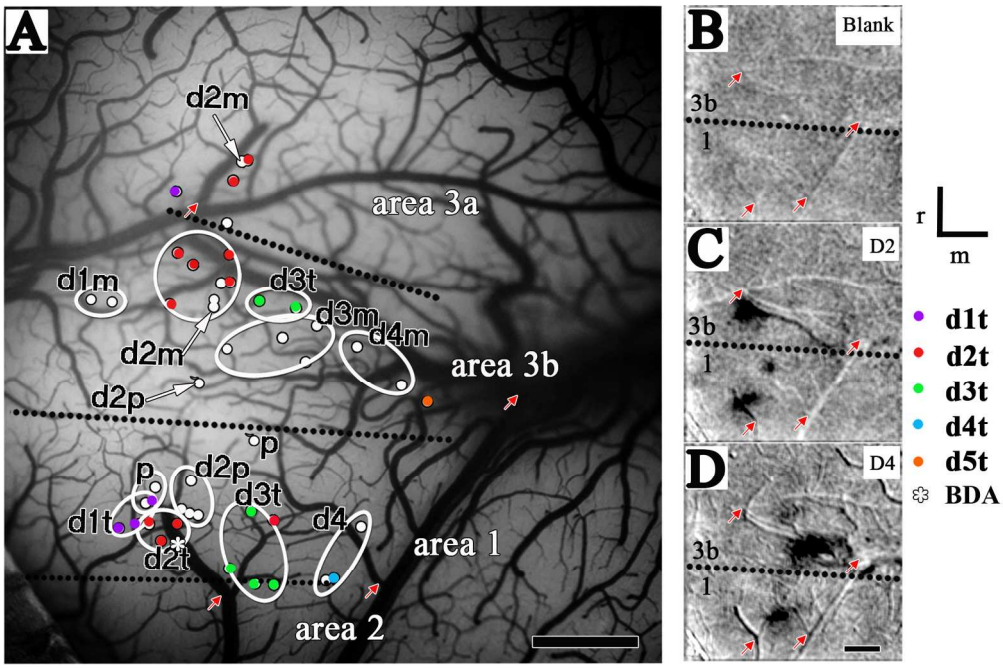


Figure 1. Mapping the glabrous part of digit representations in the somatosensory cortex with electrophysiology and optical imaging (Case M is shown). (A) Colored dots indicate electrophysiological recording sites. White ellipsoids encapsulate functional regions of similar somatotopic response preference shown also by the same color of the dots. d1-d5: digits 1-5; d1t-d5t: digit tips of fingers 1-5; d2m-d4m: middle phalanges of fingers; 2-4; d2p: proximal paert of finger 2; p: palm. The localization of BDA injection is indicated by the asterisk in the d2t region of area 1. (B) Optical image of the somatosensory cortex without stimulations. (C, D) Optical images the response of somatosensory cortex to stimulation of the D2 (C) and D4 (D) distal finger pads. Red arrows show corresponding vessel landmarks on the different images. Note the medial shift of D4 activation relative to the D2 activation sites in areas 3b and 1. Dashed lines: extrapolated borders between the areas. r: rostral, m: medial, scale bar represents 1 mm.
171x113mm (300 x 300 DPI)

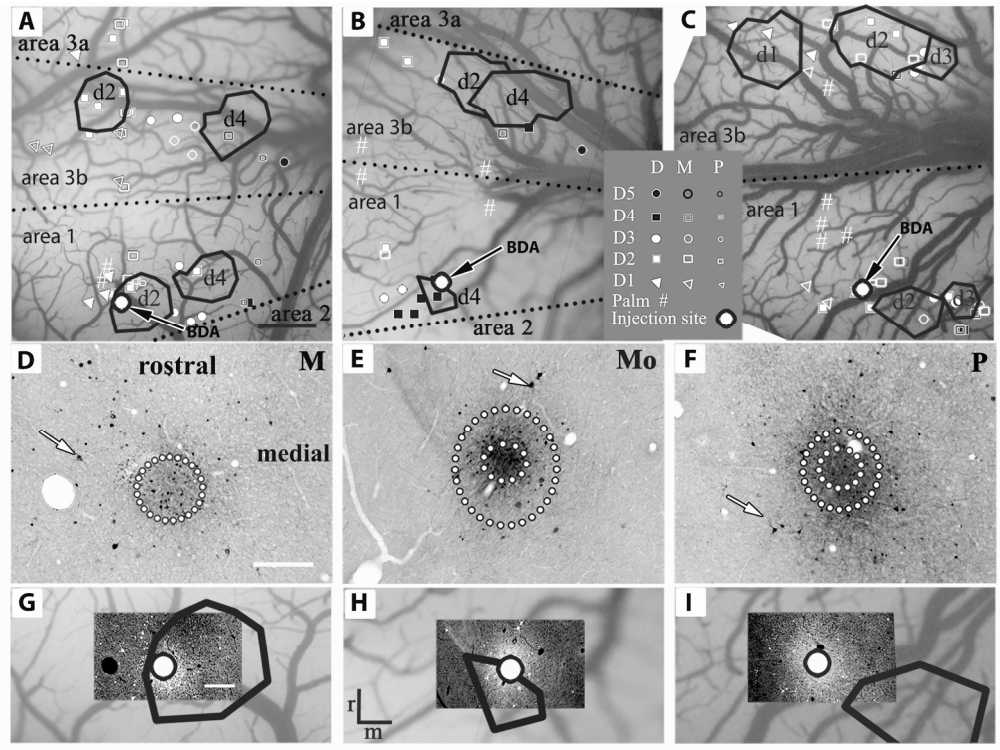


Figure 2. Localization and size of the BDA injection is shown on maps which include the electrophysiological and intrinsic optical signal (IOS) functional maps of somatosensory cortex in the three cases (M, Mo, P). (A-C) Overview of the cortical surface mapped by electrophysiology and IOS. Black outlines encircle the representation of the distal finger pad regions localized by IOS for the 3 cases. Dotted lines represent areal borders. Electrophysiological recording sites are marked by different symbols shown in the inset. (D-F) Bright field photomicrographs of the injection sites taken from the supragranular layers at a depth of 320 μm (M, Mo) and 450 μm (P) from the cortical surface. Note the core and halo organization of the BDA injection sites, which is best seen in Mo. Inner white spotted circle indicates the extent of the core, and the external circle shows the margin of the halo organization of the BDA injection. Core and halo regions could not be clearly delineated in M and P, where the highest density regions were encircled. The black holes represent cross sections of descending blood vessels (asterisk). Arrows point on BDA labeled neuronal cell bodies. (G-I) Higher magnification shows the size of the BDA injection relative to the size of the cortical area activated in the IOS experiments in the three cases. Dark field like views, where image brightness was inverted, are shown to enhance visibility. Small circle with white core: BDA injection sites; Scale bar on A represent 1 mm also applies to B and C; scale bar on D and G represent 250 μm applies also to E, F and H, I, respectively.
171x128mm (300 x 300 DPI)

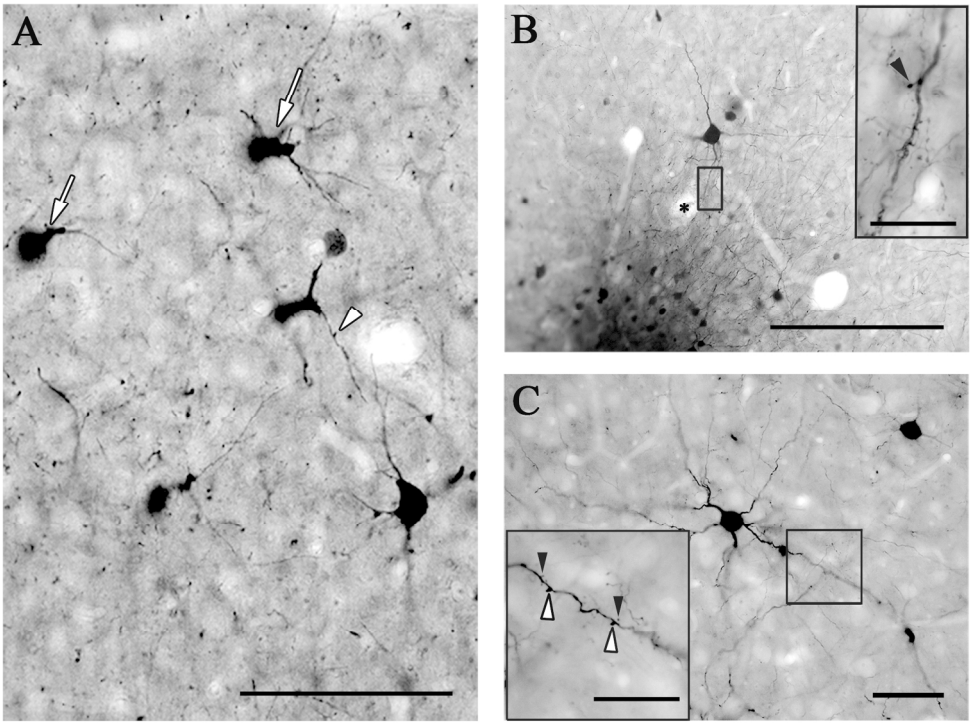


Figure 3. Retrogradely labeled neurons. (A) Pyramidal cells as identified by the appearance of the apical dendrites down the focal depth. White arrows indicate cross sections of the apical dendrites. Arrowhead: a horizontal branch originating from the apical dendrite with a protrusion. (B) A pyramidal neuron can be seen in the vicinity of the injection site (dark area in the bottom). Asterisk indicates an electrode track made during the electrophysiological mapping. Framed region is enlarged in the inset showing dendritic spines (arrowhead). Note thin, varicose axonal fiber bending around a blood vessel cut across (white "hole"). (C) Pyramidal cell with widely branching basal dendrites in the supragranular layer. Spiny dendritic spines (black arrowheads) and protrusions (white arrowheads) appear on higher magnification of the framed region in the inset. Scale bars represent 100 μm on (A), 50 μm on (B, C) and 25 μm in the inset.
171x128mm (300 x 300 DPI)

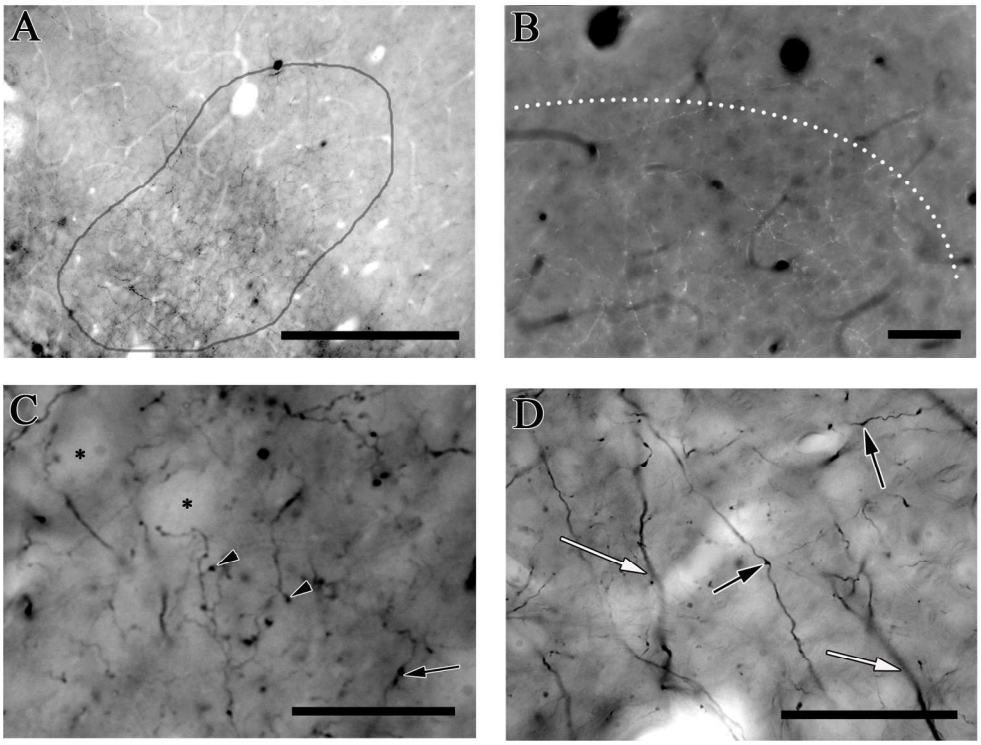


Figure 4. Anterograde labeling. (A) Pale contour outlines a terminal patch of axonal arborizations. Note the low number of retrogradely labeled neurons (appearing as black dots) within the patch. The diagonal dark stripe is a chatter of the vibratome sectioning. (B) Dotted line shows the border between the patch (lower left) and the neighboring region with low density BDA labeling. (C) Higher magnification reveals the presence of numerous thin fibers decorated by bouton-like structures. Arrowheads show terminal-like ending with stalk, arrow indicates varicosity. Asterisks mark unlabeled neuronal cell bodies partially surrounded by thin axons. (D) Long range horizontal axonal fibers with (black arrows) and without (white arrows) bouton-like varicosities (black and white arrows, respectively). Note the thick and smooth appearance of the fiber shown by the white arrow. Scale bars represent 250 μm on (A), 50 μm on (B, D) and 25 μm on (C).
171x131mm (300 x 300 DPI)

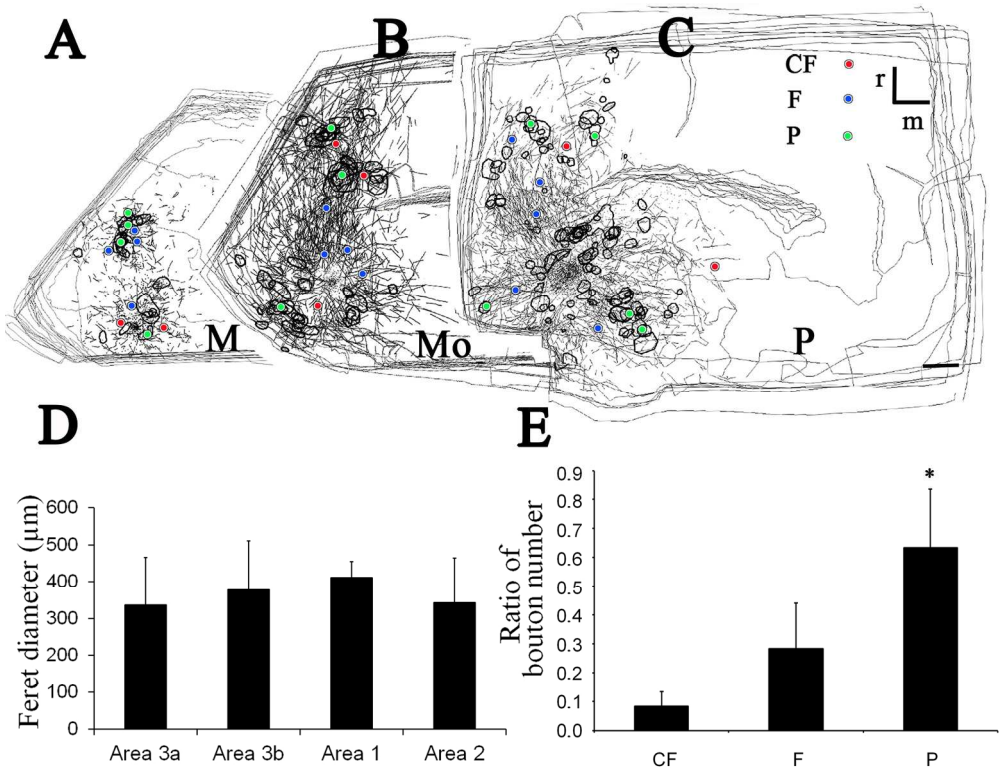


Figure 5. Size of terminal patches and density of bouton-like structures. (A-C) Overall distribution of the regions sampled for bouton density analysis on the two-dimensional reconstructions of the retrograde and anterograde labeling in M, Mo and P. Fibers are indicated by light gray curves and patches are marked by circular outlines. Black dots: retrogradely labeled neurons. CF: cell free region, F: fiber tracts and P: terminal patches. (D) Average patch size in the different cortical areas (1, 3b, 3a and 2). (E) The ratio (relative to the total counts in each case) of the average number of bouton-like structures is shown within the three different sampled regions (CF, F, P). Asterisk marks significant difference both from CF and F regions. Error bars indicate standard deviations. Scale bar represents 1 mm.
171x133mm (300 x 300 DPI)

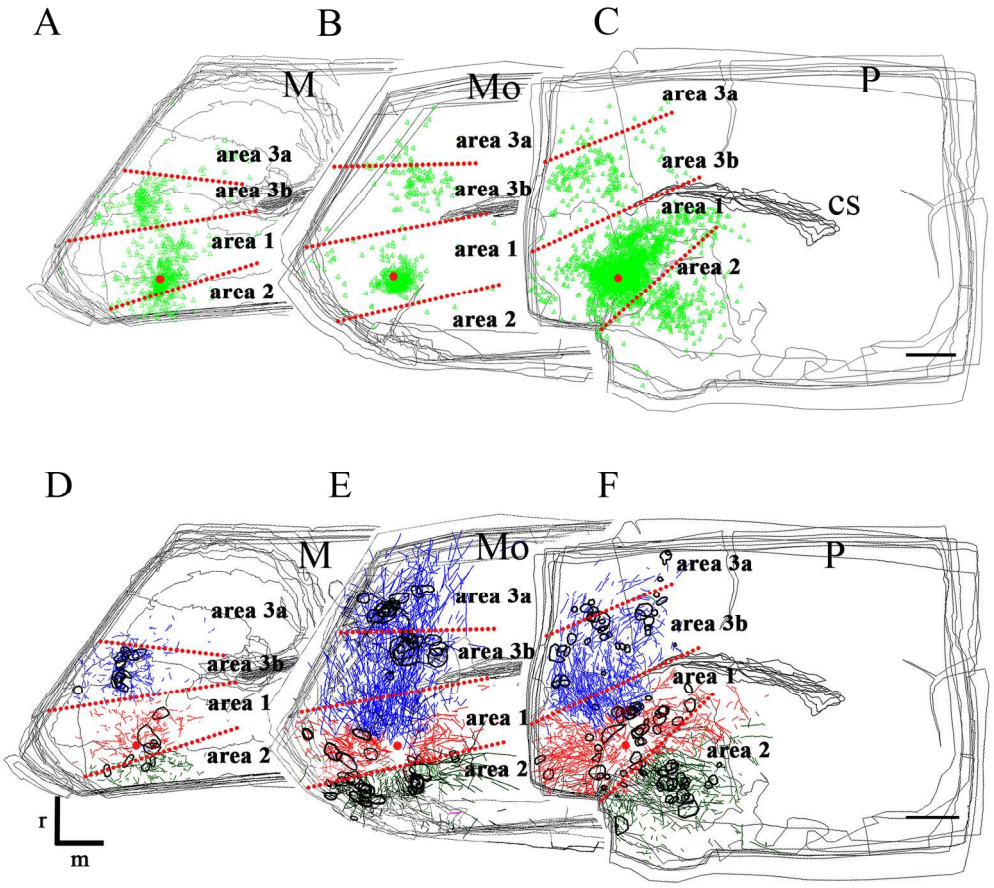


Figure 6. Retrograde and anterograde labeling in the three cases (M, Mo and P). (A-C) Distribution of retrograde labeling. Green triangles: retrogradely labeled neurons. Injection sites are marked by red dots. (D-F) Distributions of the anterograde labeling. Black outlines show terminal axon arborizations. Red lines: intrinsic connections, green lines: connections with area 2 and blue shows connections with areas 3b and 3a and perhaps M1. Red dotted lines represent areal borders. CS: central sulcus. Scale bars represent 1 mm. r: rostral, m: medial.
171x154mm (300 x 300 DPI)

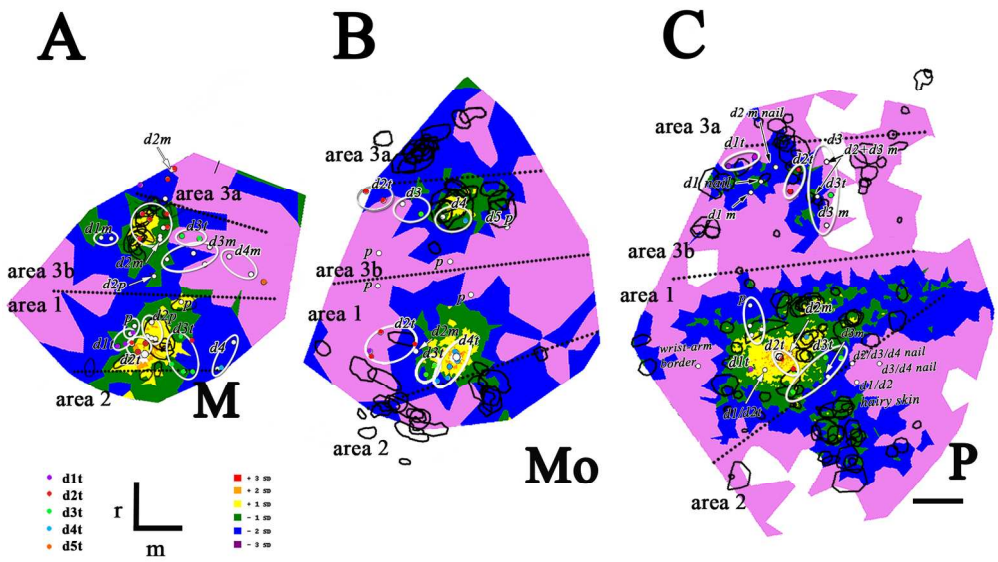


Figure 7. Alignment of the distribution of the terminal axon arborizations, the retrograde density plots and the functional electrophysiological maps. Color code for retrograde labeling density is given in units of standard deviation (SD) above and below average (for further details please see the Data analysis subsection). Dashed lines represent extrapolated borders between the areas. Colored dots indicate electrophysiological recording sites. White ellipsoids encapsulate functional regions of similar somatotopic response preference. d1-d5: digits 1-5; d1t-d5t: digit tips of fingers 1-5, d2m-d4m: middle phalanges of fingers 1-5; p: palm. Large white dots with black outline: injection site. White region around the injection site shows the area omitted from the analyses (250-300 μm diameter). r: rostral, m: medial, scale bar represents 1 mm.
171x101mm (300 x 300 DPI)

For Review

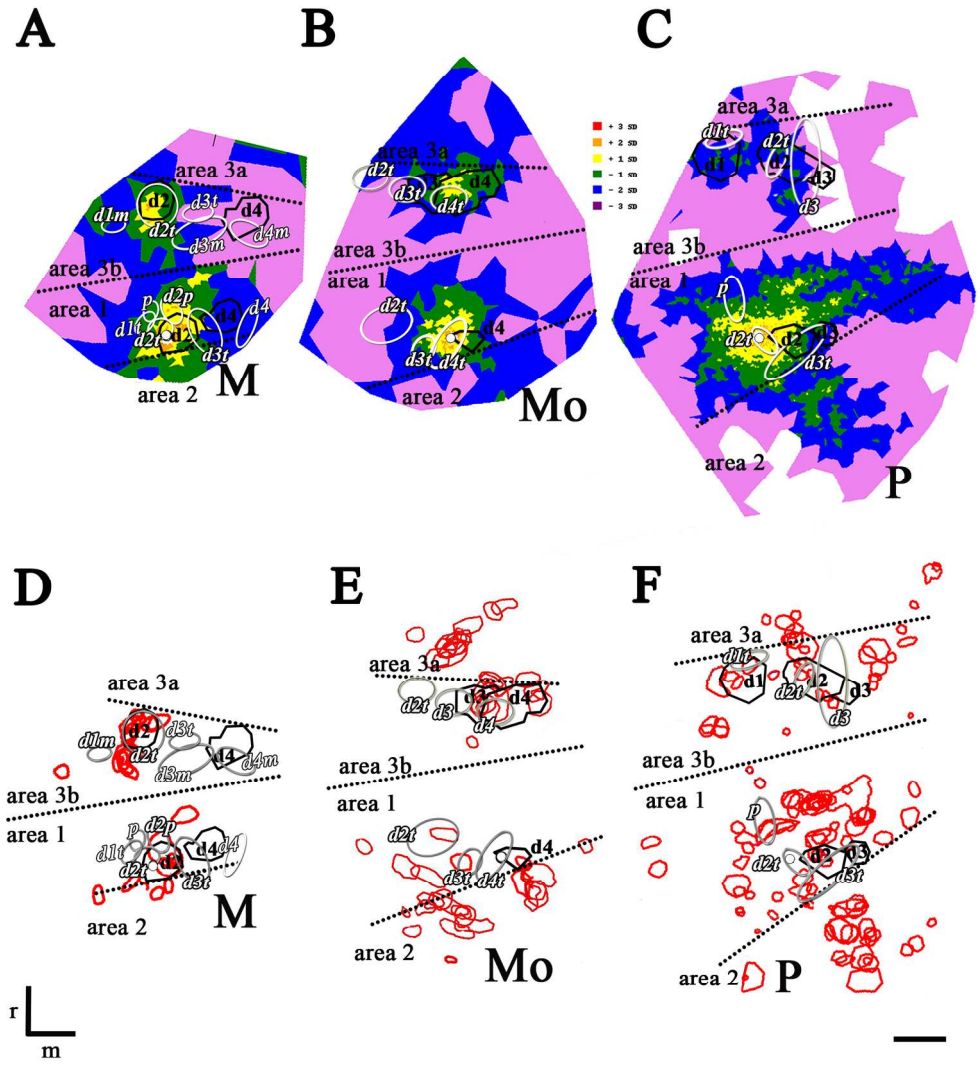
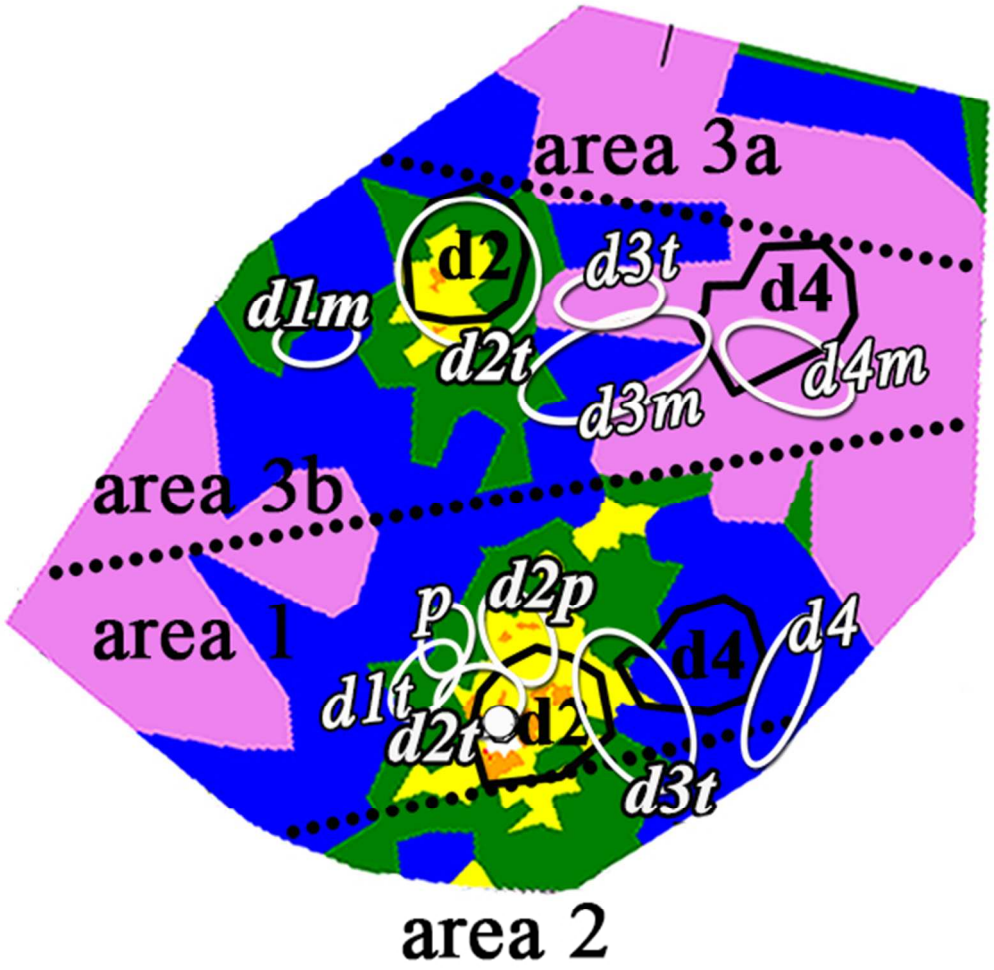


Figure 8. Alignments of the structural and functional maps in the three cases. (A-C) Input preference is shown by projecting the electrophysiological (pale outlines) and intrinsic optical signal (black outlines) maps on the 2 dimensional density plots of the retrograde labeling. (D-F) Target preference is defined by aligning the terminal patches (red outlines) with the functional maps. Conventions are the same as in Figure 7. Scale bar represents 1 mm.
171x190mm (300 x 300 DPI)



Based on anatomical, optical imaging and electrophysiological methods the authors show that intrinsic connections of area 1 connect neighboring distal finger pad representations, whereas their inter-areal connections create strong connections with homotopic regions. Connections of area 1 distal pad regions spread into more proximal representation of the fingers.
49x50mm (300 x 300 DPI)

Graphical abstract

Based on anatomical, optical imaging and electrophysiological methods the authors show that intrinsic connections of area 1 connect neighboring distal finger pad representations, whereas their inter-areal connections create strong connections with homotopic regions. Connections of area 1 distal pad regions spread into more proximal representation of the fingers.

For Peer Review



The distal finger pads of the primate hand play a fundamental role in dexterous functions controlled by the cerebral cortex. The hand has multiple, detailed, and topographically organized representations in the somatosensory cortex. The image shows the distribution of neuronal connections (green markers and yellow lines) of the cortical representation of the distal finger pad overlain on an image of the hand of the squirrel monkey. Neuronal connections form the neural substrate both for integrating multi-digit information via connecting neighboring distal finger pad representations within an area as well as for transmitting digit specific information between the neighboring somatosensory cortical areas by connecting homologous representations. This orthogonal pattern of neuronal connectivity (perpendicular and parallel with the longitudinal axes of the fingers, respectively) of the somatosensory cortex subserves the first steps of tactile cortical processing.
170x198mm (300 x 300 DPI)